NASA/TM–20250010927

Design Guidance for Filleting of Selective Laser Melted Metal Parts

Devin E. Burns
Langley Research Center, Hampton, Virginia

Vasyl Hafiychuk, Halyna Hafiychuk
KBR Inc, Ames Research Center, Mountain View, California

Kevin R. Wheeler
Ames Research Center, Mountain View, California

December 2025

NASA STI Program Report Series

Since its founding, NASA has been dedicated to the advancement of aeronautics and space science. The NASA scientific and technical information (STI) program plays a key part in helping NASA maintain this important role.

The NASA STI Program operates under the auspices of the Agency Chief Information Officer. It collects, organizes, provides for archiving, and disseminates NASA's STI. The NASA STI Program provides access to the NTRS Registered and its public interface, the NASA Technical Report Server, thus providing one of the largest collections of aeronautical and space science STI in the world. Results are published in both non-NASA channels and by NASA in the NASA STI Report Series, which includes the following report types:

- TECHNICAL PUBLICATION. Reports of completed research or a major significant phase of research that present the results of NASA programs and include extensive data or theoretical analysis. Includes compilations of significant scientific and technical data and information deemed to be of continuing reference value. NASA counterpart of peer-reviewed formal professional papers, but having less stringent limitations on manuscript length and extent of graphic presentations.
- TECHNICAL MEMORANDUM. Scientific and technical findings that are preliminary or of specialized interest, e.g., quick release reports, working papers, and bibliographies that contain minimal annotation. Does not contain extensive analysis.
- CONTRACTOR REPORT. Scientific and technical findings by NASA-sponsored contractors and grantees.
- CONFERENCE PUBLICATION. Collected papers from scientific and technical conferences, symposia, seminars, or other meetings sponsored or co-sponsored by NASA.
- SPECIAL PUBLICATION. Scientific, technical, or historical information from NASA programs, projects, and missions, often concerned with subjects having substantial public interest.
- TECHNICAL TRANSLATION. English-language translations of foreign scientific and technical material pertinent to NASA's mission.

Specialized services also include organizing and publishing research results, distributing specialized research announcements and feeds, providing information desk and personal search support, and enabling data exchange services.

For more information about the NASA STI Program, see the following:

- Access the NASA STI program home page at `http://www.sti.nasa.gov`
- Help desk contact information: `https://www.sti.nasa.gov/sti-contact-form/` and select the "General" help request type.

NASA/TM–20250010927

Design Guidance for Filleting of Selective Laser Melted Metal Parts

Devin E. Burns
Langley Research Center, Hampton, Virginia

Vasyl Hafiychuk, Halyna Hafiychuk
KBR Inc, Ames Research Center, Mountain View, California

Kevin R. Wheeler
Ames Research Center, Mountain View, California

National Aeronautics and
Space Administration

Langley Research Center
Hampton, Virginia 23681-2199

December 2025

Available from:

NASA STI Program / Mail Stop 150
NASA Langley Research Center
Hampton, VA 23681-2199

Abstract

This study used computational and experimental methods to assess the impact of a variety of fillet parameters (type, overhang length) on residual stress induced deformation in metal selective laser melted parts. Modelling results indicated increasing amounts of residual stress induced deformation with increasing unsupported overhang length. Eliminating unsupported overhang length by using large sweeping fillets was found to be an optimal strategy for reducing residual stress induced deformation and for reducing stress concentration. Computational and experimental results indicated elliptical fillets are preferred relative to circular fillets, because they reduce the amount of unsupported overhang length. Finally, introducing a tangent line when a circular or elliptical fillet becomes unsupported (to create what we call a self-supporting fillet) was found to be an effective strategy for minimizing residual stress induced deformation and should be used when unsupported overhang length becomes large.

1 Introduction

This work was driven by our interest to better understand the origin of a defect discovered in several additively manufactured wind tunnel balances. More details regarding the defect can be found in a previously published paper [1]. As this technical memorandum will detail, the defect was attributed to filleting practices used for the wind tunnel balance.

Fillets are used to facilitate geometric transitions within mechanical structures. They play an important role in mechanical design because stress concentration is heavily influenced by the type and size of fillet used. Circular fillets are widely used in traditional manufacturing because they are easy to produce with ball-end milling tools, but they do not produce optimal stress distribution. Variable radius fillets have demonstrated superior performance in reducing stress concentrations, though their adoption has been limited in conventional machining due to the increased complexity required to manufacture them. Laser powder bed fusion (LPBF) provides a pathway to incorporate advanced fillet geometries without many of the complexities associated with conventional manufacturing techniques.

Minimizing stress concentration using variable radius fillets has been studied for many decades first using photoelasticity techniques [2] and more recently with finite element modelling techniques [3, 4]. In R.B. Heywood's 1969 work [2], he defines a "streamline, ideal, or neutral fillet as one whose curvature is varied in such a manner that a uniform stress is obtained along the entire length of the fillet boundary." In practice, obtaining uniform stress along the entire length of a fillet boundary is more aspirational than practical, but the benefits of variable radius fillets can be significant.

One of the challenges of producing fillets with LPBF are the unsupported overhangs that can be created during fabrication [5–7]. As the fillet progresses to an overhang angle of 45 degrees, it becomes unsupported and undesirable amounts of residual stresses can develop. Residual stresses become more pronounced in unsupported areas because the gradient of the heating and cooling rates increases locally as the layer of powder to be melted transitions from being supported by solid material to being supported by powder. In general, there is a direct relationship between the size of the unsupported overhang and the amount of residual stress and therefore localized deflection [5]. This study looks to better quantify this relationship for different fillet geometries. Two common geometries used in mechanical structures are studied: standalone fillets and two merged fillets that form a bridge like structure (hereafter referred to as bridge fillets). For both standalone and bridge fillets, we investigate three different fillet types: circular, elliptical, and self-supporting. Both additive thermal simulations and a confirmation build were used to gain insight into the effect of fillet geometry on residual stress induced deformation and ultimately to make recommendations about filleting best practices for LPBF.

2 Methods

2.1 Computational Methods

Ansys 2025/R2 software was used to simulate residual stress induced deformation in Ti-6Al-4V additively manufactured parts, which is currently the material used for production additively manufactured wind tunnel balances. The simulation followed a layer-by-layer solidification approach mirroring the additive manufacturing process.

Thermal (temperature) and structural (distortion and stress) physics were treated as largely uncoupled. First, we performed a thermal simulation on a per-layer basis to capture the temperature evolution throughout the build (parts being built, build plate, and surrounding air). The build was assumed to start at room temperature and temperature changes were captured through cooling down of the part after completion of the build. These temperature results were then used as input for a subsequent structural simulation to evaluate distortion and residual stress.

In additive manufacturing simulation, the model evolves over time as new material layers are added to replicate the real build process. The entire part was initially meshed using a layered mesh (either Cartesian or tetrahedral). We then employed the standard element birth and death technique to activate element layers sequentially, simulating the progressive build.

Boundary conditions, such as thermal convection surfaces, were also updated dynamically throughout the simulation. The first layer is assumed to be rigidly attached to the build plate. The build step was considered complete once all element layers were activated. Analysis times and time stepping were governed by process parameters and determined automatically by the solver during the simulation.

In this report, we present the directional deformation results and compare them with experimental data. Residual stress results are not included, as no corresponding experimental measurements were available for validation.

2.2 Experimental Methods

Several fillets were printed on a SLM 280 printer using Ti-6Al-4V powder. Standard print parameters recommended by the manufacturer were used and are summarized in Table 1. The fillet coupons were designed such that each fillet completed printing at the same build height as illustrated in Figure 1. The print ended one layer after the fillets were completed. Only a single print was completed.

Table 1: Print parameters used for the confirmation build.

Layer thickness	60 µm
Power	950 W
Scan Speed	230 mm/s
Hatch Spacing	0.1 mm

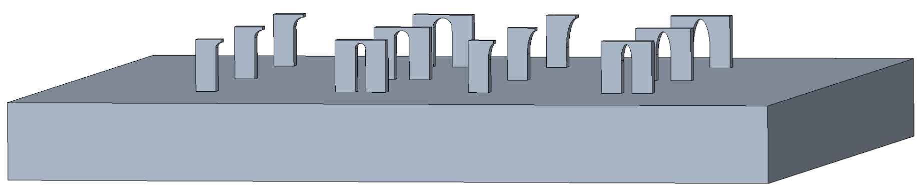

Figure 1: Isotropic view of the fillet coupons positioned on the build plate.

Deformation measurements were made with a white light interferometer (Keyence VR 6200). Several line profiles were averaged across the surface to reduce the noise due to individual solidified melt pools.

3 Results and Discussion

Ansys additive simulation tools were initially used to model the wind tunnel balance that resulted in the defect discussed in the Introduction. Figure 2 shows a computer aided design representation of the entire wind tunnel balance and calls out what is referred to as the cage section where the defect was found. Simulations of the additive build process focused on the cage section (Figure 3 a)) showed the highest amounts of predicted residual stress induced deformation at the general location where the defect was observed (Figure 3 b)). In this region, beam elements transition into a bulkhead via fillets. A close inspection of the fillets suggests that the deformation becomes particularly pronounced as the fillets become unsupported. Based on these results, it is our hypothesis that unsupported overhang areas were a contributing factor to the formation of the defect likely due to localized deformation in that area leading to a recoater interference issue.

To test this hypothesis, we changed the geometry that transitioned the one beam element into the bulkhead. While the original geometry used a elliptical fillet, we

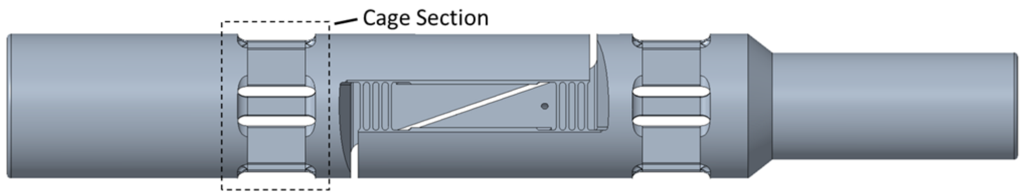

Figure 2: Wind tunnel balance highlighting the cage section geometry that is modeled in this section.

inserted an even larger elliptical fillet that eliminated the overhang all together as shown in Figure 3 c). Ansys additive simulations of the large elliptical fillet showed a significant reduction in the total deformation (Figure 3 d)) predicted in these regions. The use of large radii that never become unsupported appears to be an optimal solution from both a stress concentration and additive residual stress perspective. However, it is not practical to assume that such large radii can always be implemented. As a result, the remainder of the study investigated fillets with varying amounts of overhang.

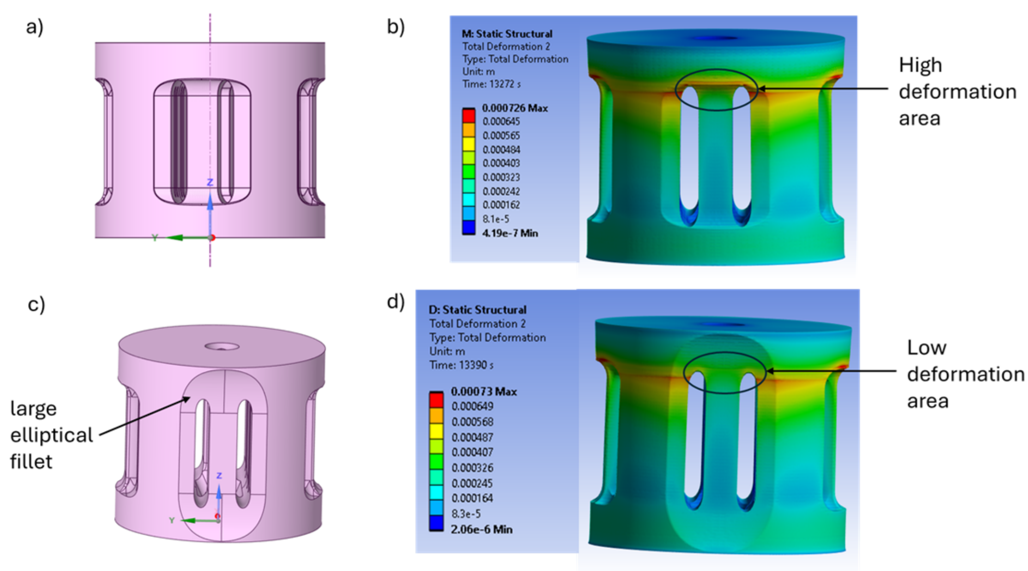

Figure 3: a) Geometry of the wind tunnel balance with observed defect and b) predicted deformation. c) Geometry of modified wind tunnel balance fillet and d) predicted deformation.

While the wind tunnel balance cage geometry study was insightful to the likely cause of the experimental defect observed in the previous work, it was unnecessary to model such a complex structure as we sought to better understand filleting best practices. As a result, simpler standalone fillet coupons were used for the remainder of the work.

3.1 Fillet Simulations

The circular, elliptical, and self-supporting fillets investigated in this study are shown in Figure 4. A self-supporting fillet is a modification of a circular or elliptical fillet where a tangent line is drawn to complete the fillet after an overhang angle of 45 degrees has been reached. The self-supporting fillets reported on in this study are modified circular fillets. A composite image showing all the fillets superimposed on one another is also shown in Figure 4 to provide perspective on how the different fillets effect the amount of overhang. Several fillet sizes were investigated, but we will primarily report on fillets 0.125" in length since this was determined to be an upper bound with respect to fillets used for wind tunnel balance cage sections. Additionally, several elliptical major to minor axis ratios were investigated, but we will report on major to minor axis ratios of three since this ratio is close to the minimum with respect to stress concentration.

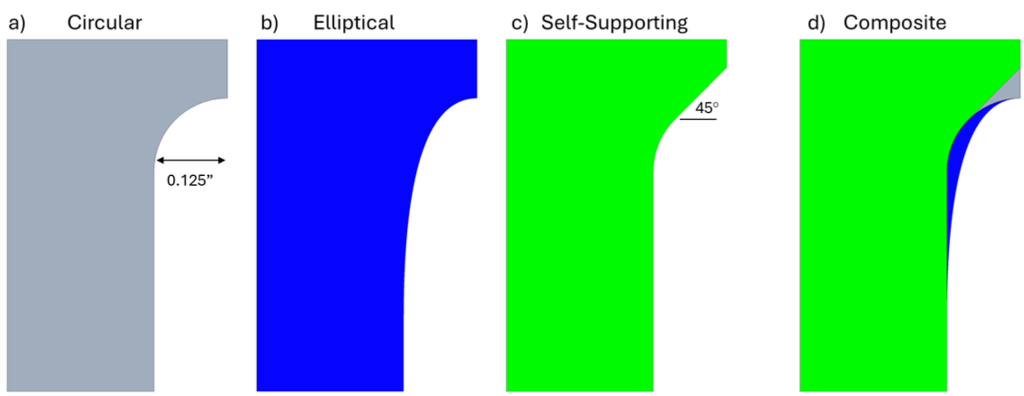

Figure 4: Illustrations of fillets modelled in this study including a) circular b) elliptical c) self-supporting and d) a composite image showing the fillets superimposed on one another.

Ansys additive simulation results for the three fillet types (Figure 5) showed larger vertical deformation and thus greater potential for recoater interference with increasing unsupported overhang distance. The circular fillet (Figure 5 a)) had the largest overhang and therefore the largest amount of vertical deformation with the highest potential for recoater interference. The elliptical fillet (Figure 5 b)) with its modest overhang length had a much less pronounced vertical deformation compared to the circular fillet. Finally, the self-supporting fillet with no overhang length exhibited the least vertical deformation on the final printed layer.

It is important to note that for all the simulation results the majority of the top surface starts at a deformation of approximately -0.050 mm. Deformation of the individual point measurements noted in Figure 5 a)-c) are reported relative to an assumed -0.050 mm reference plane for consistency.

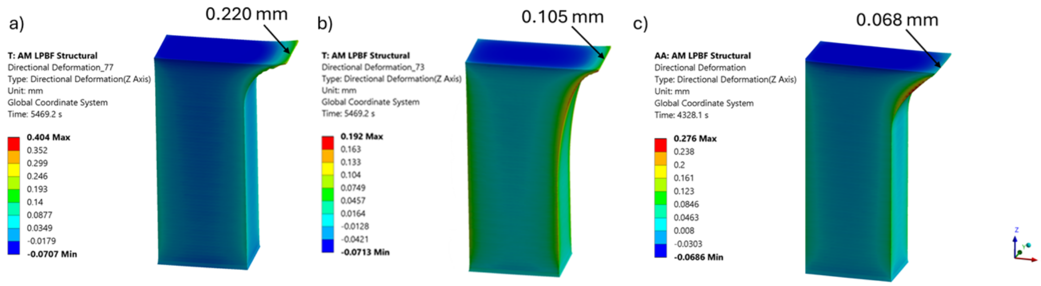

Figure 5: Predictions of residual stress induced deformation for a) circular, b) elliptical, and c) self supporting fillets.

3.2 Bridge Simulations

Two fillets coming together to form bridge like structures are a common occurrence as part of wind tunnel balance geometries and many other structures. Much like the fillets discussed in the previous section we sought to characterize the residual stress induced deformation for circular, elliptical, and self-supporting bridge structures (Figure 6). While we looked at a number of different bridge spans we present results for a total bridge span of 0.25" (0.125" for each fillet), since this is generally considered an upper bound for balance cage section geometries. Similarly, we again focus on an elliptical fillet with a major to minor axis ratio of three.

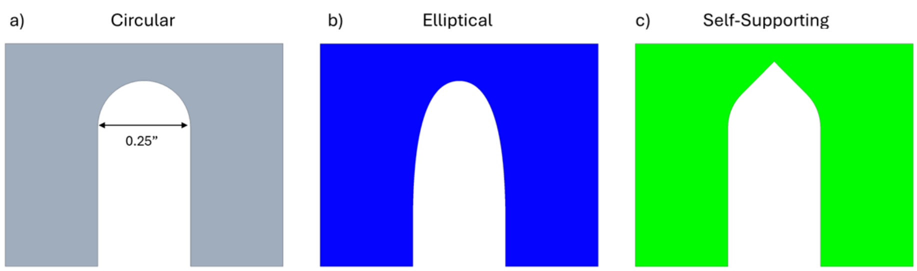

Figure 6: Illustrations of bridges modelled in this study including a) circular b) elliptical and c) self-supporting.

Vertical deformation predictions are presented in Figure 7 for the a) circular b) elliptical and c) self-supporting bridge structures. Once again all point deformation results reported in Figure 7 were relative to a reference plane of -0.050 mm. Like the fillet simulations for the bridges the largest predicted deformation occurred for the circular bridge structures followed by elliptical and self-supporting bridge structures. And in general, the bridge simulations showed less predicted vertical deformation than the fillet simulations. This suggests that fillets deserve particular attention during the model design process and that bridge structures appear a little more forgiving.

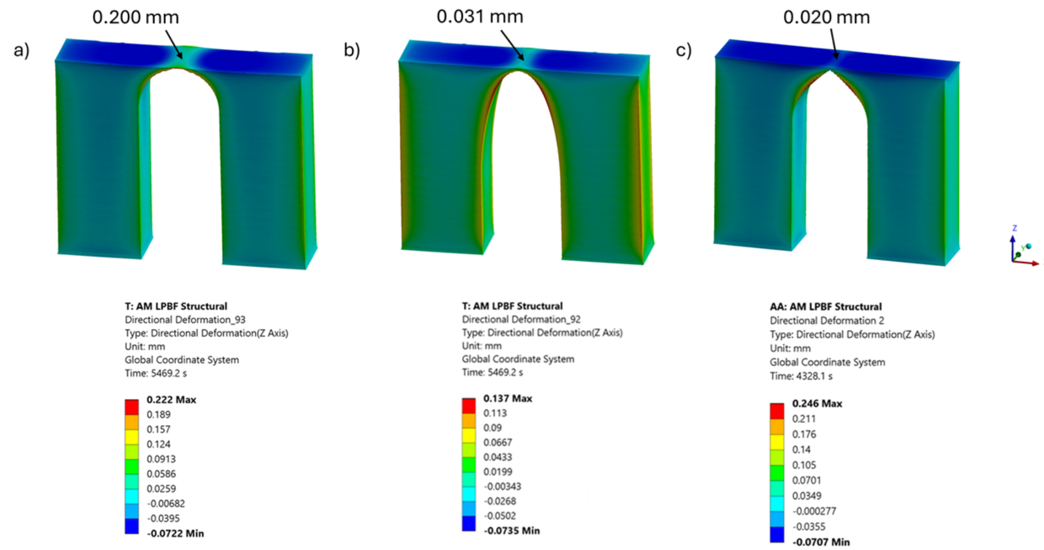

Figure 7: Predictions of residual stress induced deformation for a) circular, b) elliptical, and c) self supporting bridges.

3.3 Experimental Validation

As depicted in Figure 1, a number of fillet and bridge structures were printed to compare predicted residual stress induced vertical deformation with actual deformation observed in practice. A white light interferometer was used to measure deformation along the top surface of the coupons producing surface deformation maps like that shown in Figure 8 a). Individual line displacement profiles were taken across the surface as illustrated in Figure 8 b) where each white line represents an individual profile. The individual line displacement profiles were averaged creating the average line displacement profile shown in Figure 8 c). Total deformation was then estimated by subtracting an established flat reference baseline from the peak displacement value as illustrated by the annotations in Figure 8 c).

The predicted and measured deformations are compared in Table 2 for 0.1" and 0.125" circular and elliptical fillets. Experimental validation of the self-supporting geometries was not completed due to time and budget limitations, but would be nice to complete in the future. The predicted deformation results provided clearer takeaways than the measured deformation results. For instance, the 0.125" elliptical and circular fillets had larger predicted deformations than the smaller 0.1" fillets consistent with our expectations. Moreoever, the predicted elliptical deformation was consistently smaller than the predicted circular deformation. The one measured data point we have for the 0.125" elliptical fillet indicates that the ratio of the elliptical to circular deformation is approximately 0.5 consistent with our predictions.

While the ratio of the circular to elliptical deformation was generally consistent for both the predicted and measured cases, the measured deformations were approximately half of the predicted deformations. Several factors may have con-

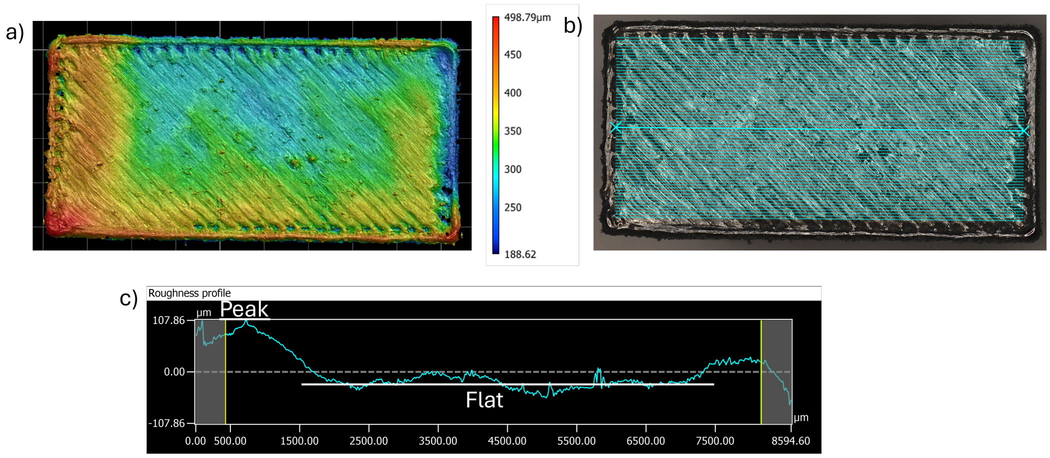

Figure 8: a) Surface deformation map b) Individual lines used for profile averaging c) Surface deformation results based on line averaging.

tributed to the larger predicted deformations. One of these factors includes the models accounting of heat accumulation and dissipation. Overhangs are prone to heat buildup due to limited thermal contact with the bulk part below. Heat must dissipate through less efficient paths—support structures and the surrounding powder bed. The Ansys model may overestimate temperature gradients in these regions, leading to higher predicted thermal stresses and exaggerated upward curling (positive z-deformation). Accurately modeling powder thermal conductivity is especially challenging, as it varies with temperature and degree of consolidation. Moreover, melt pool dynamics maybe impacting the predicted deformations. The melt pool's size and stability often differs on overhangs versus well-supported regions, affecting solidification and residual stress development. If the simulation's heat source model does not fully capture these effects, it can misrepresent layer-by-layer stress accumulation.

Note that the measurements were taken on the as-printed surface, which included a fair amount of roughness impacting our ability to resolve residual stress induced deformation. This likely contributed to our inability to measure deformations for the 0.1" elliptical fillet. It may also help explain why we measured a larger deformation for the 0.1" circular fillet relative to the 0.125" circular fillet. In the future, polishing the top surface prior to interferometer measurement should improve the signal to noise ratio and thus improve measurement resolution.

Table 2: Predicted and measured vertical deformations for several fillets.

Fillet Type	Predicted Deformation (mm)	Measured Deformation (mm)
0.1" circular	0.190	0.130
0.1" elliptical	0.100	Not measurable
0.125" circular	0.230	0.120
0.125" elliptical	0.110	0.060

Model predictions of the deformation of the bridge structures were not consistent with experimental results. The modelling results consistently predicted a lifting of the unsupported area similar to the fillets. In reality, the bridge structures sagged in the unsupported area. This is consistent with other experimental work where the top layer of a hole was found to sag into the unsupported area below it [5, 8]. The discrepancy can likely be attributed in part to the fact that the simulations do not include the effects of gravity. In addition, the models accounting of heat accumulation and dissipation and the melt pool dynamics likely play a role as well as discussed above.

4 Conclusions

The results suggest that additional work is required to improve the accuracy of the modelling results particularly for the bridge structures. Despite modeling limitations, the collective results point to the following design guidance when filleting AM structures:

1. Eliminate overhangs if possible using larger fillets.

2. Elliptical fillets are preferred over circular fillets from both a residual stress and stress concentration standpoint.

3. If overhangs become to large, implementing self-supporting circular or elliptical fillets is an effective method to reduce residual stress induced deformation.

References

1. Devin E. Burns and Eric R. Burke. A case study for qualification of a structural additively manufactured one-off component. *The International Journal of Advanced Manufacturing Technology*, 136(3):1587–1596, 2025.

2. R.B. Heywood. *Photoelasticity for Designers.* Pergamon Press, 1969.

3. Jaime Tupiassú Pinho de Castro, Daniel de Albuquerque Simões, Ivan Fabio Mota de Menezes, Marco Antonio Meggiolaro, and Luiz Fernando Martha. A note on notch shape optimization to minimize stress concentration effects. *Theoretical and Applied Fracture Mechanics*, 84:72–85, 2016. Notch Mechanics.

4. Xueqiang Wang, Siping Li, and Liming Peng. A structural curve with reduced stress concentration and its elastic–plastic failure analysis. *Engineering Failure Analysis*, 162:108339, 2024.

5. Daniel Thomas. *The Development of Design Rules for Selective Laser Melting.* PhD thesis, University of Wales Institute, Cardiff, 2009.

6. Guido A. O. Adam and Detmar Zimmer. On design for additive manufacturing: evaluating geometrical limitations. *Rapid Prototyping Journal*, 21(6):662–670, 10 2015.

7. Chance P. Garcia, Shawn W. Skinner, Omar R. Mireles, Paul R. Gradl, Robin Osborne, and Jonathan Harris. *Metal Additive Manufacturing for Propulsion Applications*, chapter 7, pages 439–526. American Institute of Aeronautics and Astronautics, 2022.

8. Shaochuan Feng, Shijie Chen, Amar M. Kamat, Ru Zhang, Mingji Huang, and Liangcai Hu. Investigation on shape deviation of horizontal interior circular channels fabricated by laser powder bed fusion. *Additive Manufacturing*, 36:101585, 2020.